Mapping global leaf inclination angle (LIA) based on field measurement data

Sijia Li[1,2,3], Hongliang Fang[1,2]

[1]LREIS, Institute of Geographic Sciences and Natural Resources Research, Chinese Academy of Sciences, Beijing 100101, China
[2]College of Resources and Environment, University of Chinese Academy of Sciences, Beijing 100049, China
[3]National-Local Joint Engineering Laboratory of Geo-Spatial Information Technology, Hunan University of Science and Technology, Xiangtan 411201, China.

Correspondence to: Sijia Li (lisj.19b@igsnrr.ac.cn)

Abstract. Leaf inclination angle (LIA), the angle between leaf surface normal and zenith directions, is a vital trait in radiative transfer, rainfall interception, evapotranspiration, photosynthesis, and hydrological processes. Due to the difficulty in obtaining large-scale field measurement data, LIA is typically assumed to follow the spherical leaf distribution or simply considered constant for different plant types. However, the appropriateness of these simplifications and the global LIA distribution are still unknown. This study compiled global LIA measurements and generated the first global 500 m mean LIA (MLA) product by gap-filling the LIA measurement data using a random forest regressor. Different generation strategies were employed for noncrops and crops. The MLA product was evaluated by validating the nadir leaf projection function (G(0)) derived from the MLA product with high-resolution reference data. The global MLA is 41.47°±9.55°, and the value increases with latitude. The MLAs for different vegetation types follow the order of cereal crops (54.65°) > broadleaf crops (52.35°) > deciduous needleleaf forest (50.05°) > shrubland (49.23°) > evergreen needleleaf forest (47.13°) ≈ grassland (47.12°) > deciduous broadleaf forest (41.23°) > evergreen broadleaf forest (34.40°). Cross-validation shows that the predicted MLA presents a medium consistency ($r = 0.75$, RMSE = 7.15°) with the validation samples for noncrops, whereas crops show relatively lower correspondence ($r = 0.48$ and 0.60 for broadleaf crops and cereal crops) because of limited LIA measurements and strong seasonality. The global G(0) distribution is opposite to that of the MLA and agrees moderately with the reference data ($r = 0.62$, RMSE = 0.15). This study shows that the common spherical and constant LIA assumptions may underestimate the intercept capability for most vegetation. The MLA and G(0) products derived in this study would enhance our knowledge about global LIA and should greatly facilitate remote sensing retrieval and land surface modeling studies.

The global MLA and G(0) products can be accessed at:

Li, S. and Fang, H. 2024, https://doi.org/10.5281/zenodo.10940673.

1 Introduction

Vegetation regulates terrestrial carbon and water cycles through a series of biophysical processes such as photosynthesis, respiration, and transpiration (Foley et al., 1996; Chen et al., 2019). These biophysical processes are mainly carried by leaves and the characterization of leaves within canopies is vital for remote sensing and earth system modeling (Ross, 1975; Lawrence et al., 2019). Leaf inclination angle (LIA) denotes the inclination of the leaf or needle to the horizontal plane or the angle between the leaf surface normal and zenith (Wilson, 1960). LIA is a key canopy structural trait that determines radiative transfer, rainfall interception, evapotranspiration, photosynthesis, and hydrological processes (Sellers, 1985; Ross, 1981; Mantilla-Perez and Salas Fernandez, 2017; Xiao et al., 2000; Maes and Steppe, 2012). LIA has been used in radiative transfer modeling (RTM), remote sensing inversion, and land surface modeling (LSM) studies (Tang et al., 2016; Wang and Fang, 2020; Lawrence et al., 2019; Ross, 1975).

At the canopy scale, the probability density of LIA or the fraction of leaf area per unit LIA is expressed as the leaf angle distribution (LAD) (De Wit, 1965). De Wit (1965) summarized six theoretical LADs, including planophile, erectophile, extremophile, plagiophile, uniform, and spherical distributions. Specifically, the spherical distribution assumes that the relative probability density of the LIA is proportional to the area of the corresponding sphere surface element and its mean leaf inclination angle (MLA) equals 57.3° (MLA = 57.3°) (De Wit, 1965). Furthermore, Ross (1981) defined the inclination index (χ_L) to describe the departure of LAD from the spherical distribution. For the planophile distribution, $\chi_L = 1$; for the erectophile distribution, $\chi_L = -1$; and for the spherical distribution, $\chi_L = 0$. In the radiative transfer regime, LIA is generally represented by the leaf projection function ($G(\theta)$), which is defined as the average projection ratio of unit leaf area in the illumination or viewing direction θ (Ross, 1981; Nilson, 1971). The spherical distribution is characterized by an isotropic leaf projection function ($G \equiv 0.5$) (De Wit, 1965).

In the field, LIA can be measured directly based on the leaf's geometrical structure or using indirect optical methods (Lang, 1973; Ryu et al., 2010; Norman and Campbell, 1989; Weiss and Baret, 2017). Using these methods, several LIA measurements have been carried out and some LIA datasets were constructed (Kattge et al., 2020; Chianucci et al., 2018; Hinojo-Hinojo and Goulden, 2020; Pisek and Adamson, 2020). These field methods are usually time-consuming and labor-intensive and are typically difficult to acquire large-scale LIA (Li et al., 2023). In addition, the existing LIA datasets have not been comprehensively analyzed. LIA has also been estimated from satellite imagery through empirical relationships or radiative transfer model inversions (Zou and Mõttus, 2015; Bayat et al., 2018; Goel and Thompson, 1984). Remote sensing methods are used primarily for crops in local regions, and the generality of these algorithms is limited (Li et al., 2023). Due to the difficulty in large-scale LIA measurements and estimations, our knowledge about the global LIA remains lacking.

Because our understanding of the global LIA is limited, different LIA simplification strategies have been adopted in various studies. For example, LIA is typically assumed to follow the spherical distribution (Tang et al., 2016; Zhao et al., 2020; Wang and Fang, 2020). However, this assumption may decrease the accuracy of radiative transfer modeling, significantly underestimate the radiation interception (Stadt and Lieffers, 2000), and cause large errors (>50%) in leaf area index (LAI) measurements and inversions (Yan et al., 2021). The spherical LIA assumption may introduce greater error in the nadir direction than other viewing geometries (Yan et al., 2021), considering the large G variation in this direction (Wilson, 1959). The lack of global LIA knowledge also limits the retrieval of other vegetation structural parameters(Li et al., 2023). In many LSMs, LIA is commonly treated as a fixed value for different plant function types (PFT) (Lawrence et al., 2019; Majasalmi and Bright, 2019). Field LIA measurements have demonstrated that the spherical distribution is not appropriate for forests, and the PFT-dependent LIA ignores LIA variation within the PFT (Pisek et al., 2013; Yan et al., 2021; Majasalmi and Bright, 2019).

This study aims to generate the first global MLA map from existing LIA field measurements using a data-driven gap-filling method. This method involves spatial expansion and upscaling of LIA measurements, and a random forest regressor using input spectral, climate, and PFT data. Based on the global MLA map, we tested whether the spherical LIA assumption is appropriate at the global scale. The new MLA map was validated by comparing the nadir G (G(0)) derived from the MLA with high-resolution reference data. Section 2 outlines the materials and methods employed to generate and evaluate the global MLA. Section 3 presents the global LIA measurements, global MLA and G(0), and evaluation results. Section 4 discusses the performance of the global MLA and G(0), the usage of the new MLA map, and the limitations of the study. Section 5 presents the main conclusions.

2 Materials and methods

2.1 LIA measurement data

2.1.1 TRY LIA dataset

TRY is a network of vegetation scientists headed by Future Earth, the Max Planck Institute for Biogeochemistry, and German Centre for Integrative Biodiversity Research, providing a global database of curated plant traits (the TRY database) (https://www.trydb.org/TryWeb/Home.php). Since its establishment in 2007, the TRY database has continuously evolved and has become one of the most widely used vegetation trait databases. The latest V6 version (released on October 13, 2022) employed in this study contains 15,409,681 trait records covering 305,594 plant taxa (Kattge et al., 2020). In this database, LIA was recorded as a numerical or categorical variable. After data extraction and checking, 31,043 valid records were used, which include numerical LIA, locations, and species. Many measurements lack location information, whereas, for some locations, there are many measurements for individual species. The spatial distribution map appears relatively sparse despite a large volume of data (Fig. 1). The LIA measurements in South America are mainly from palms.

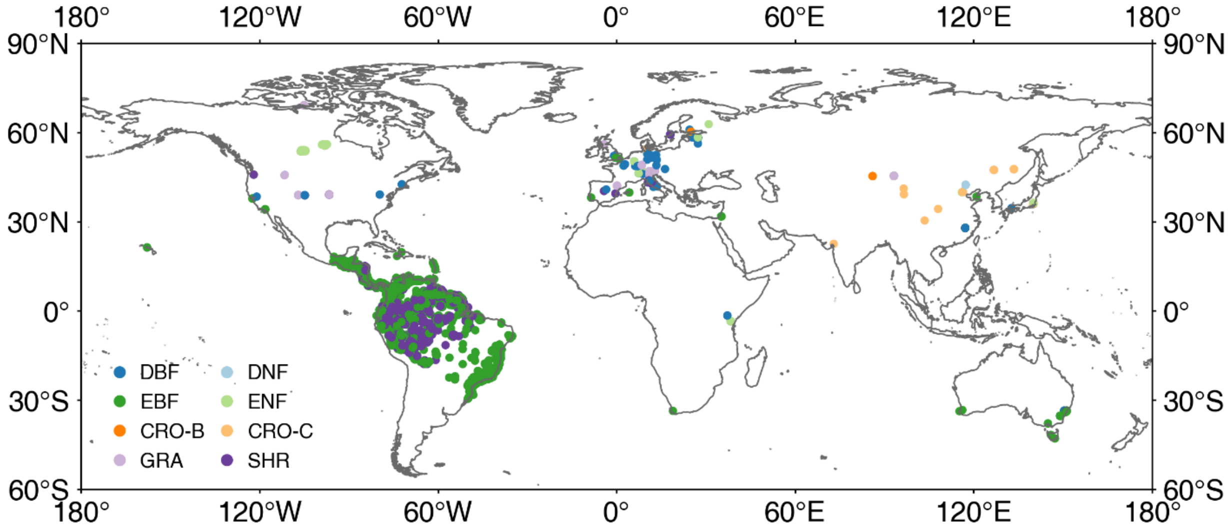

Figure 1. The locations of global leaf inclination angle measurements. DBF: deciduous broadleaf forest, DNF: deciduous needleleaf forest, EBF: evergreen broadleaf forest, ENF: evergreen needleleaf forest, CRO-B: broadleaf crops, CRO-C: cereal crops, GRA: grassland, SHR: shrubland.

2.1.2 LIA data from the literature

The LIA measurements in published literature were collected via keyword search (leaf angle, leaf inclination angle, and leaf tilt angle) in the Web of Science, Google Scholar, Google, and Chinese documentary databases. The LIA, location, and species information were manually extracted from the literature (Fig. 1). Several LIA measurements were already included in the TRY database (Chianucci et al., 2018; Pisek and Adamson, 2020). After aggregating LIA measurements for the same species at the same location, 780 LIA records were accessed from previous studies (Hinojo-Hinojo and Goulden, 2020; Pisek et al., 2022; Chen et al., 2021).

2.1.3 Manual LIA extraction

Only a few measurements in the northern tundra region were obtained, and the measurements in tropical regions are dominated by palm trees (Fig. 1). Therefore, LIA data for the northern tundra and tropical regions were extracted from horizontal side-view photographs searched from Google (Fig. S1).

ImageJ software (https://imagej.nih.gov/ij/) was used to process the leveled photographs and derive LIA following the method of Pisek et al. (2011). The TRY species location data (848,919, Fig. S3b) (Jan 03, 2022) were used to obtain the dominant species information in tropical rainforests and the northern tundra. The species location points in these two vegetation types were spatially filtered and the frequency of occurrence for each species was counted. The species with a high frequency of occurrence were selected to measure the LIA. For each species, more than 75 leaves perpendicular to the viewing direction were selected and processed based on visual judgment to ensure the stability and reliability of the MLA (Pisek et al., 2013). In total, the MLA of 104 species was manually derived.

In this study, most LIA measurements are obtained with protractor and level digital photogrammetry, especially for needleleaf species. Therefore, the distinction between branches and leaves is considered. The diverse LIA records from different sources were sorted to match the TRY species and to get the PFT based on the TRY Categorical Traits Dataset 2018 (https://www.try-db.org/TryWeb/Data.php#3). The MLA was calculated for the LIA records with different forms. If there were multiple LIA records for the same species, the mean value was computed for the same location and species. In total, 5,554 LIA records of 1,194 species were collected, covering the growing season from 2001 to 2022. LIA location replicates per species range from 1 to 330, and most replicates (98 %) are less than 50. Considering the different numbers of records for each species, the LIA data was further aggregated by species.

2.2 Remote sensing data

2.2.1 Ancillary data used for MLA mapping

The ancillary data used for global MLA mapping and analysis are listed in Table 1. The PFT classification system in the MODIS global 500 m land cover type product (MCD12Q1.061) was used and mode-aggregated from 2001 to 2022 to match the LIA measurements (Fig. S2) (Sulla-Menashe et al., 2019). The 2001–2022 Landsat surface reflectance (Level 2, Collection 2, Tier 1) (Crawford et al., 2023), including Landsat 5 (2001–2012), Landsat 7 (2012–2013), and Landsat 8 (2013–2022) was utilized to generate a global 30 m PFT map (Section 2.3.1), which was subsequently employed for LIA upscaling. The 2001–2022 MODIS bidirectional reflectance distribution function (BRDF) model parameters dataset (MCD43A1 C6.1) (Schaaf and Wang, 2015a) and nadir BRDF adjusted reflectance dataset (MCD43A4 V6 NBAR) (Schaaf and Wang, 2015b) are produced daily using 16 days of Terra and Aqua MODIS data at 500 m resolution and were utilized as predictive variables. Due to the scarcity of crop LIAs and the lack of location information for existing crop LIA measurements, fine-resolution (10/30 m) crop-type maps (Table 1) in 2018 were employed to support crop LIA mapping. Other data include the ERA5-Land reanalysis data, the ALOS digital elevation model (AW3D30 V3.2), and the 2001–2022 MODIS LAI product (MCD15A2H) (Myneni, 2015). The LAI product was averaged and aggregated from 2001–2022. Most earth observation data were accessed and processed in Google Earth Engine (GEE) (https://earthengine.google.com/).

Table 1. Remote sensing data for global MLA mapping. BRDF: bidirectional reflectance distribution function.

Category	Data	Year	Spatial resolution	Temporal resolution	Reference
Plant function type	MCD12Q1 C6	2001–2022	500 m	Yearly	(Sulla-Menashe et al., 2019)
Surface reflectance	Landsat collection 2	2001–2022	30 m	16 days	(Crawford et al., 2023)
	MCD43A4 V6 NBAR	2001–2022	500 m	Daily	(Schaaf and Wang, 2015b)
BRDF	MCD43A1 C6.1	2001–2022	500 m	Daily	(Schaaf and Wang, 2015a)
Crop type	Cropland Data Layers (CDL)	2018	30 m	Yearly	(Boryan et al., 2011)

	EUCROPMAP	2018	10 m	Yearly	(D’andrimont et al., 2021)
	AAFC Annual Crop Inventory	2018	30 m	Yearly	(Fisette et al., 2013)
	Northeast China crop-type map	2018	30 m	Yearly	(You et al., 2021)
	NESEA-Rice10	2018	10 m	Yearly	(Han et al., 2021)
	China maize map	2018	30 m	Yearly	(Shen et al., 2022)
	China winter wheat map	2018	30 m	Yearly	(Dong et al., 2020)
Climate	ERA5-Land	2001–2022	0.1°	Monthly	(Muñoz-Sabater et al., 2021)
Terrain	AW3D30 V3.2	—	30 m	—	(Tadono et al., 2014)

2.2.2 High-resolution reference data

The high-resolution reference datasets provided by Ground Based Observations for Validation (GBOV, https://land.copernicus.eu/global/gbov/dataaccessLP/) and DIRECT 2.1 (https://calvalportal.ceos.org/lpv-direct-v2.1) were used to evaluate the generated global MLA (Fig. 2). These datasets provide high-resolution (20/30 m) LAI, effective LAI (LAIe), and fractional vegetation cover (FVC) data over a 3 km × 3 km area centered on each site generated using empirical relationships between various vegetation indices and ground measurements (Li et al., 2022; Brown et al., 2020). GBOV has provided continuous high-resolution reference data since 2013 (Fig. 2).

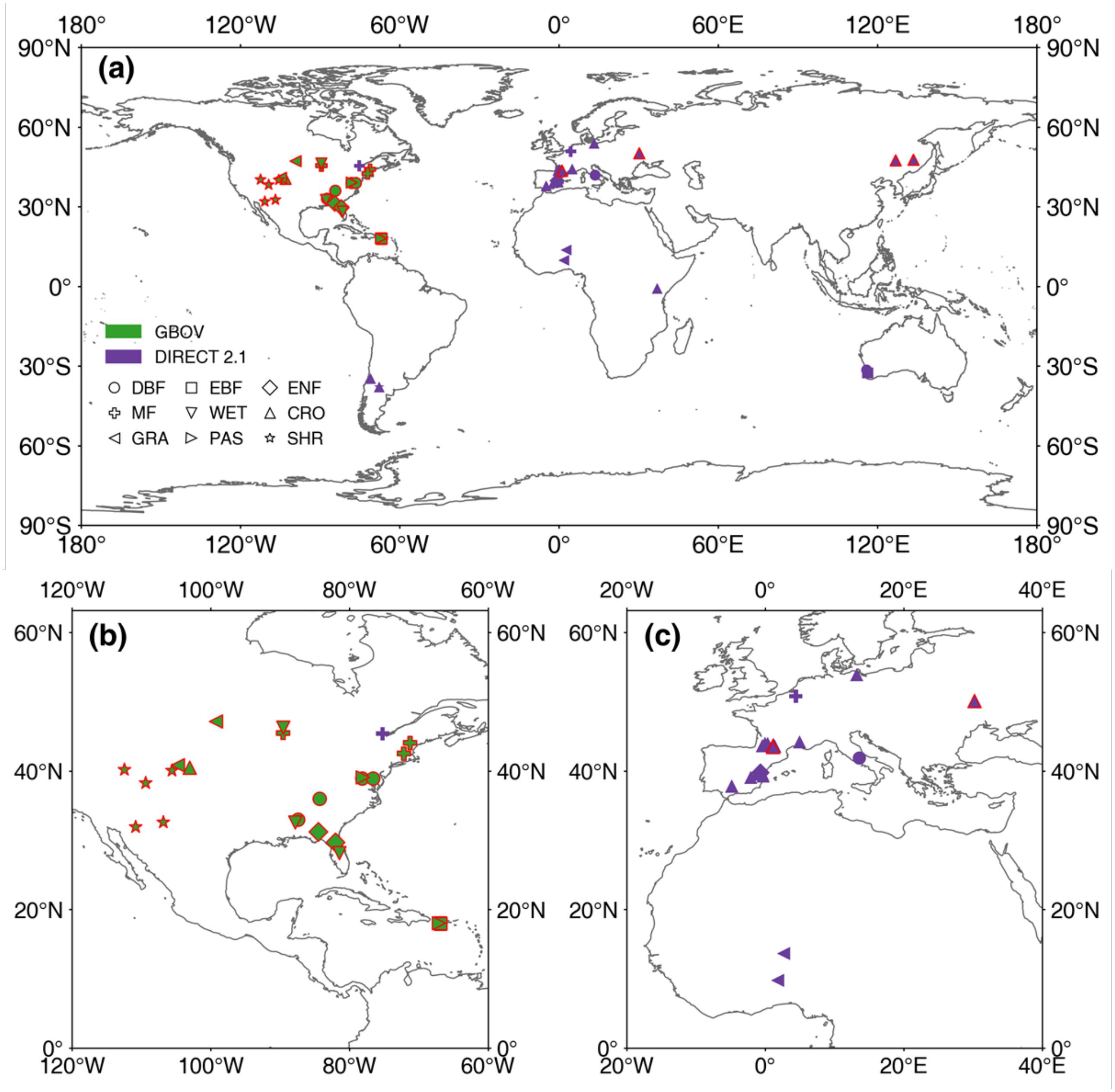

Figure 2. Locations of GBOV and DIRECT 2.1 sites used in this study (a). (b) and (c) show the sites in North America and Europe, respectively. CRO: Cultivated crops, MF: Mixed forest, PAS: Pasture/hay, WET: Woody wetlands. See Fig. 1 for other acronyms. The red frame indicates those sites with >5 continuous records.

2.3 Mapping global LIA

2.3.1 Data preparation

Many studies have treated LIA as a species-specific static trait and ignored within-species variations when LIA measurements are limited (Pisek et al., 2022; Toda et al., 2022; Raabe et al., 2015). Following the rationale, the spatial coverage of LIA measurements was expanded, and those records without location information were utilized (section 2.1.1). Under this assumption, the LIA measurements were expanded through TRY species location data with species name matching. When a species had multiple LIA observations at different locations, the nearest LIA was assigned to the TRY species location. Visual inspections were conducted to remove potential TRY location biases, especially for non-vegetated points such as water bodies and deserts. After spatial expansion, the number of LIAs reached 12,328 (Fig. S3c).

In this study, the scale gap between field measurements and satellite remote sensing data was fully considered. To upscale the LIA measurements to the satellite resolution (500 m), a 30 m PFT map was first derived from Landsat reflectance using a random forest classification method. The random forest was trained at a 500 m scale using the mode-aggregated MODIS PFT classification map as training samples to generate a 30 m PFT map by hierarchically selecting homogeneous pixels (with a coefficient of variation in reflectance < 0.2). The classification features were the same as those in the MODIS classification algorithm (Sulla-Menashe et al., 2019). For a 500 m pixel with multiple PFTs (Fig. 3a), when one PFT had no LIA measurement, the LIA of the PFT was assigned with the value of its nearest neighbor within 100 km with the same PFT. In field measurement, the entire canopy LIA is calculated as the average of all measured leaf LIAs weighted by leaf area (Zou et al., 2014; De Wit, 1965). Leaves with larger areas have higher weights. Upscaling LIA from 30 m to 500 m follows the same rationale as that from leaf to canopy scale. For a 30 m pixel with a higher LAI, the weight of the pixel is higher. Therefore, The 500 m MLA was computed as the weighted average of the enhanced vegetation index (EVI2) considering a linear relationship between LAI and EVI2 (Dong et al., 2019; Alexandridis et al., 2019).

$$MLA_{500m} = \frac{\sum MLA_{30m} \times EVI2_{30m}}{\sum EVI2_{30m}} \qquad (1)$$

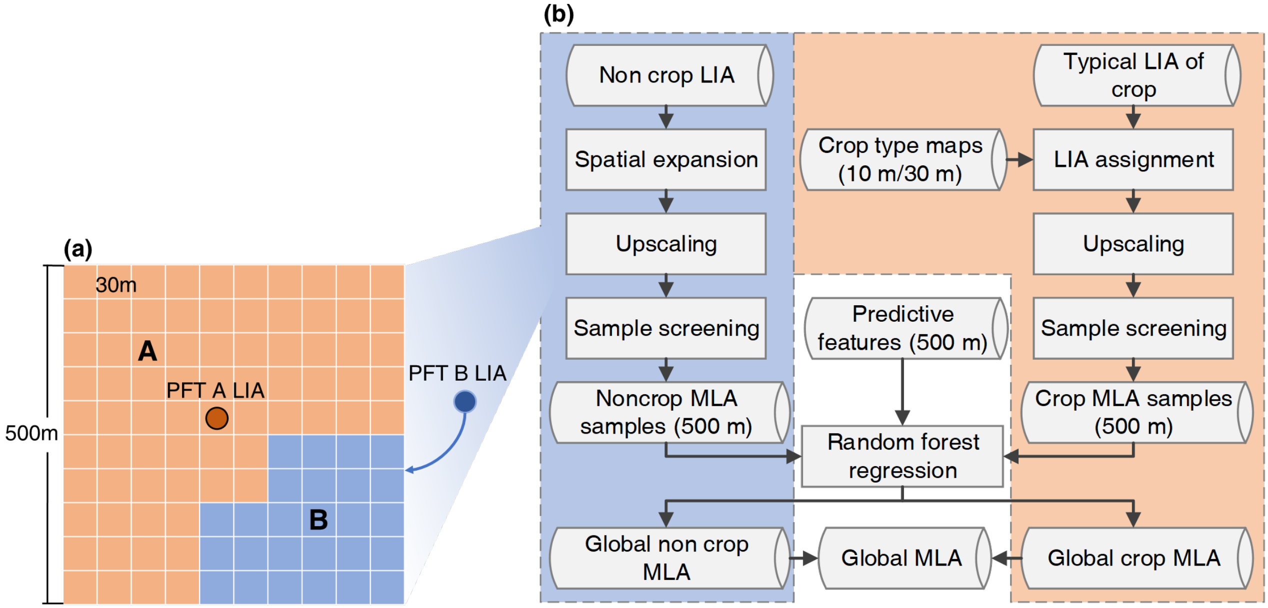

Figure 3. Leaf inclination angle (LIA) upscaling (a) and global mean LIA (MLA) mapping (b) strategies.

The 500 m upscaled MLA samples were further refined to select the most representative samples following three criteria: 1) the coefficient of variation of the 30 m EVI2 in the 500 m pixel is less than 0.2, 2) the vegetation proportion in the 500 m pixel is greater than 0.8, and 3) the proportion of PFTs represented by the MLA measurements in the 500 m pixel is greater than 0.4. The final number of samples after refinement is 3,013 (Fig. 4).

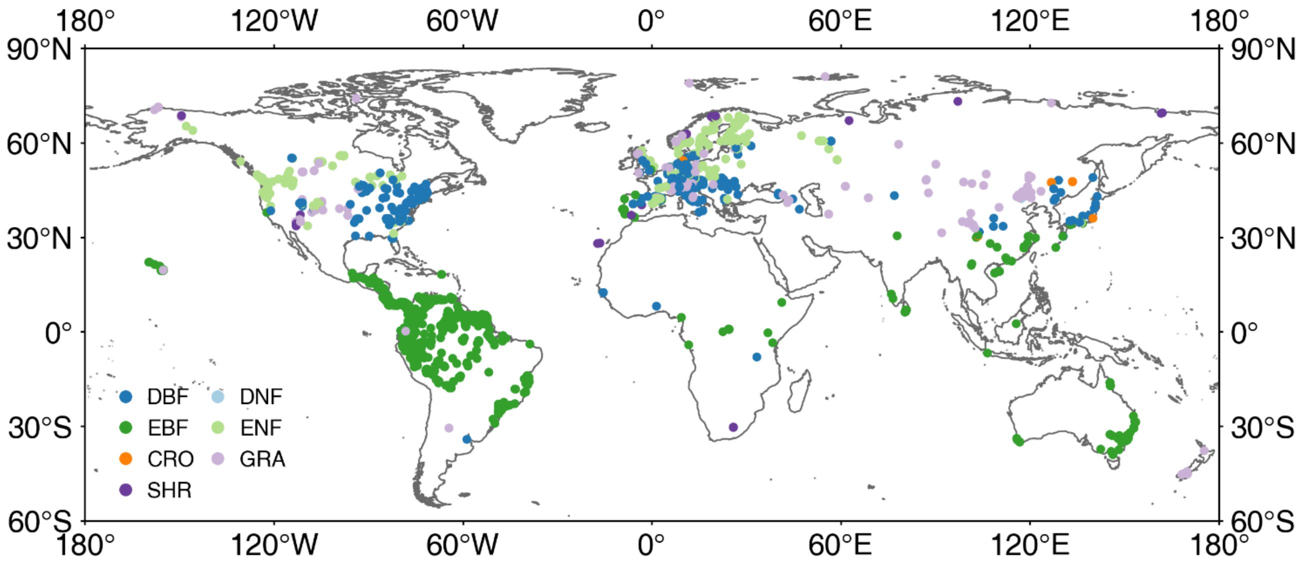

Figure 4. Distribution of global mean leaf inclination angle samples after screening. See Fig. 1 for acronyms.

2.3.2 Global MLA mapping

Different mapping strategies were employed for noncrops and crops (Fig. 3b) considering the small number of valid crop samples (Fig. 4) and the lack of location information for most crop samples. For noncrops, the upscaled 500 m MLA samples were used to train a random forest regressor to predict the global MLA from different features (Table 2). To reduce computational complexity and potential overfitting, a feature selection process was conducted based on the variable importance (the sum of the decrease in Gini impurity index over all trees in the forest) computed by the model, and only the 40 most important variables were used in the final prediction. During the training process, the out-of-bag error was minimized to obtain the optimal hyperparameters. The prediction performance of the random forest regressor was evaluated using a ten-fold cross-validation approach.

For crops, the measured MLA values were averaged for different crop types as a typical MLA (Table S2). After assigning typical MLAs for different crops with high-resolution crop maps (Table 1), the high-resolution crop MLA were upscaled to 500 m as training samples (Eq. (1)). Only the samples with a crop area ratio > 80% within a 500 m pixel were selected for training. The crops were further divided into broadleaf crops and cereal crops and processed with the same procedure used for noncrops (Fig. 3b). All procedures were conducted on GEE under the WGS-84 geographic coordinate system.

Table 2. Predictive features in global MLA mapping.

Category	Features	Variables	Number
Spectral	Blue, green, red, near-infrared reflectance	10%, 33%, 50%, 67%, 90% quantiles and standard deviation	24
	NDVI	10%, 33%, 50%, 67%, 90% quantiles and standard deviation	6
BRDF	Kernel coefficients of the red band	10%, 33%, 50%, 67%, 90% quantiles and standard deviation	18
	Kernel coefficients of near-infrared band	10%, 33%, 50%, 67%, 90% quantiles and standard deviation	18
PFT	PFT	Constant	1
Climate	Solar downward radiation	Mean and standard deviation	2
	Temperature	Mean and standard deviation	2
	Precipitation	Mean and standard deviation	2
Terrain	Elevation	Constant	1
	Slope	Constant	1
	Aspect	Constant	1

2.4 Evaluation of global MLA

The global MLA map was indirectly evaluated using the leaf projection function, limited by the lack of high-resolution reference MLA. The global G(0) was derived from the MLA and evaluated with high-resolution reference following the upscaling scheme recommended by the Land Product Validation (LPV) Subgroup of the Committee on Earth Observation

Satellites (CEOS) (http://lpvs.gsfc.nasa.gov/). The nadir G(0) is important considering that most satellite sensors adopt the nadir observation geometry.

Assuming a single-parameter ellipsoidal leaf angle distribution (Campbell, 1990; Wang et al., 2007), the parameter χ, the ratio of the horizontal and vertical axes of an ellipsoid, was first derived from MLA. Compared to other models, the single-parameter ellipsoidal leaf angle distribution is a relatively more accurate and simpler model and has been used in many remote sensing studies (Campbell, 1990; Wang et al., 2007; Kuusk, 2001; Verhoef et al., 2007).

$$\chi = -3 + \left(\frac{MLA}{9.65}\right)^{-0.6061} \tag{2}$$

The G(θ) value in the nadir direction (θ=0°) was calculated using the following analytical formula.

$$G(\theta) = \frac{\sqrt{(\chi^2 + tan^2\,\theta)}\,cos\,\theta}{\chi + 1.774(\chi + 1.182)^{-0.73}} \tag{3}$$

The reference G(0) was derived from high-resolution LAI, FVC, and clumping index (CI) (=LAIe/LAI) with the Beer-Lambert law (Fig. S4) (Nilson, 1971).

$$P(\theta) = exp^{-\frac{G(\theta)*LAI*CI(\theta)}{cos(\theta)}} \tag{4}$$

Where $P(\theta)$, $CI(\theta)$, and $G(\theta)$ denote the gap fraction, CI, and G in direction θ, respectively. Specifically, the gap fraction in the nadir direction can be expressed by FVC.

$$P(0) = 1 - FVC \tag{5}$$

Therefore, the reference G(0) was derived using the following formula.

$$G(0)\_CI(0) = -\frac{ln^{(1-FVC)}}{CI(0)*LAI} \tag{6}$$

By using the whole CI as the nadir CI (CI(0)) in the above equation (Fang et al., 2021; Li et al., 2022), G(0) was calculated as follows:

$$G(0)\_CI \approx -\frac{ln^{(1-FVC)}}{CI*LAI} \tag{7}$$

The MLA product was first upscaled to 3 km through a weighted averaging method using the MODIS LAI to derive G(0) (Eq. (3)). The reference LAI, FVC, and CI were also upscaled to 3 km through simple averaging to compute the reference G(0) (Eq. (7)). The MLA-derived G(0) and the reference G(0) were compared at the 3 km × 3 km area around each site. The correlation coefficient (*r*), bias, and root mean square error (RMSE) were calculated as the evaluation metrics, as follows:

$$r = \sqrt{1 - \frac{\sum_{i=1}^{n}(\hat{y}_i - y_i)^2}{\sum_{i=1}^{n}(y_i - \bar{y})^2}} \tag{8}$$

$$Bias = \frac{1}{n}\sum_{i=1}^{n}(\hat{y} - y_i) \tag{9}$$

$$RMSE = \sqrt{\frac{1}{n}\sum_{i=1}^{n}(\hat{y} - y_i)^2} \tag{10}$$

where $\hat{y}_i$, y_i, and n denote the MLA-derived G(0), reference G(0), and the number of G(0), respectively.

3 Results

3.1 Global measured LIA values

The species-aggregated LIA was employed in the analysis of global LIA measurements. Fig. 5 shows the distributions of global measured LIA values for different PFTs. The global measured MLA is 40.74° and generally follows the order of CRO-C > GRA > ENF > CRO-B > EBF > SHR > DNF > DBF (Table 3). Cereal crops exhibit the highest MLA (59.11°), whereas DBF has the most horizontal leaves (MLA = 34.94°). GRA and EBF show large LIA variations (Std = 20.44° and 17.17°), whereas CRO-B exhibits a small range. The DNF LIA measurements are only for one species and show very little variation (Fig. 5).

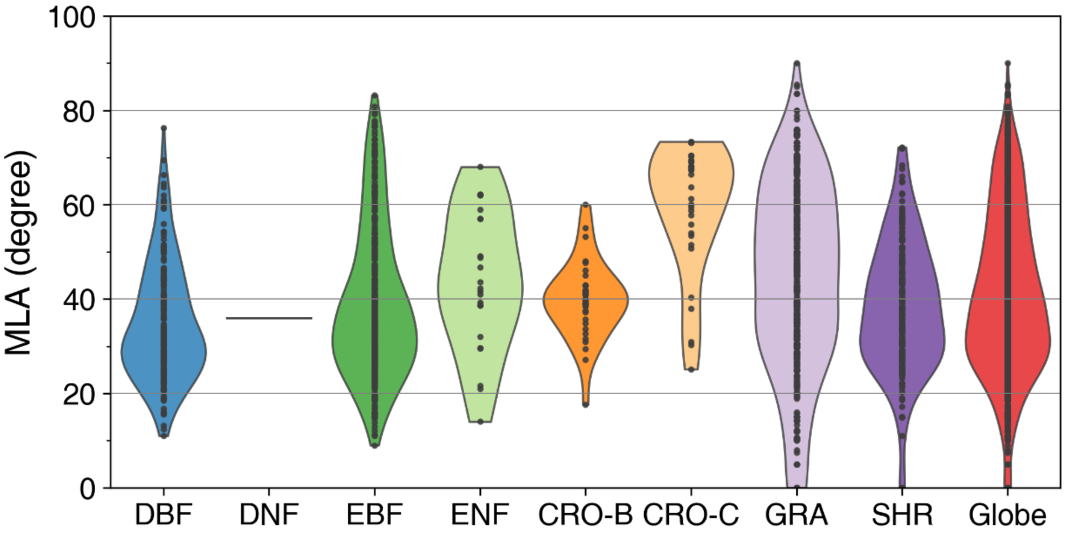

Figure 5. Distribution of global mean LIA (MLA) for different plant function types (see Fig. 1 for acronyms). The last shape shows the global average. Statistics are conducted for each species as represented by points in the figure.

Table 3. Statistics of leaf inclination angle measured for different plant functional types (PFT). STD is the standard deviation. The inclination index (χ_L) is converted from mean leaf inclination angle (MLA) ($\boldsymbol{\chi_L = 2cos(\mathrm{MLA}) - 1}$) (Lawrence et al., 2019).

PFT	DBF	DNF	EBF	ENF	CRO-B	CRO-C	GRA	SHR	Globe
Number of species	171	1	347	23	32	31	399	190	1194

Mean(°)	**34.94**	35.88	39.30	43.69	39.71	**59.11**	44.13	38.32	40.74
STD (°)	12.40	0.00	**16.11**	14.40	8.11	13.28	**20.17**	13.80	17.12
χ_L	0.64	0.62	0.55	0.45	0.54	0.03	0.44	0.57	0.52

3.2 The relationships between MLA and other variables

Fig. 6 shows the importance of the top 40 variables in the MLA prediction obtained from the random forest regression model. The importance of these 40 variables accounts for 78% of the total importance among all 76 variables. Spectral features account for 30% of the importance, which is higher than that of other features. Among the spectral features, NDVI, near-infrared (NIR) band, and red band reflectance are most critical for MLA prediction. The importance of BRDF features is comparable to that of climatic variables (21% vs. 20%), followed by terrain features (7%). Among the BRDF features, the NIR BRDF information shows a higher contribution than the red band, with importance in the following order: geometrically scattered kernel> isotropic scattering kernel > volumetric scattering kernel. The importance ranking of the climatic variables follows the order of precipitation ≈ solar radiation > temperature. Additionally, elevation shows a considerable impact on the MLA prediction.

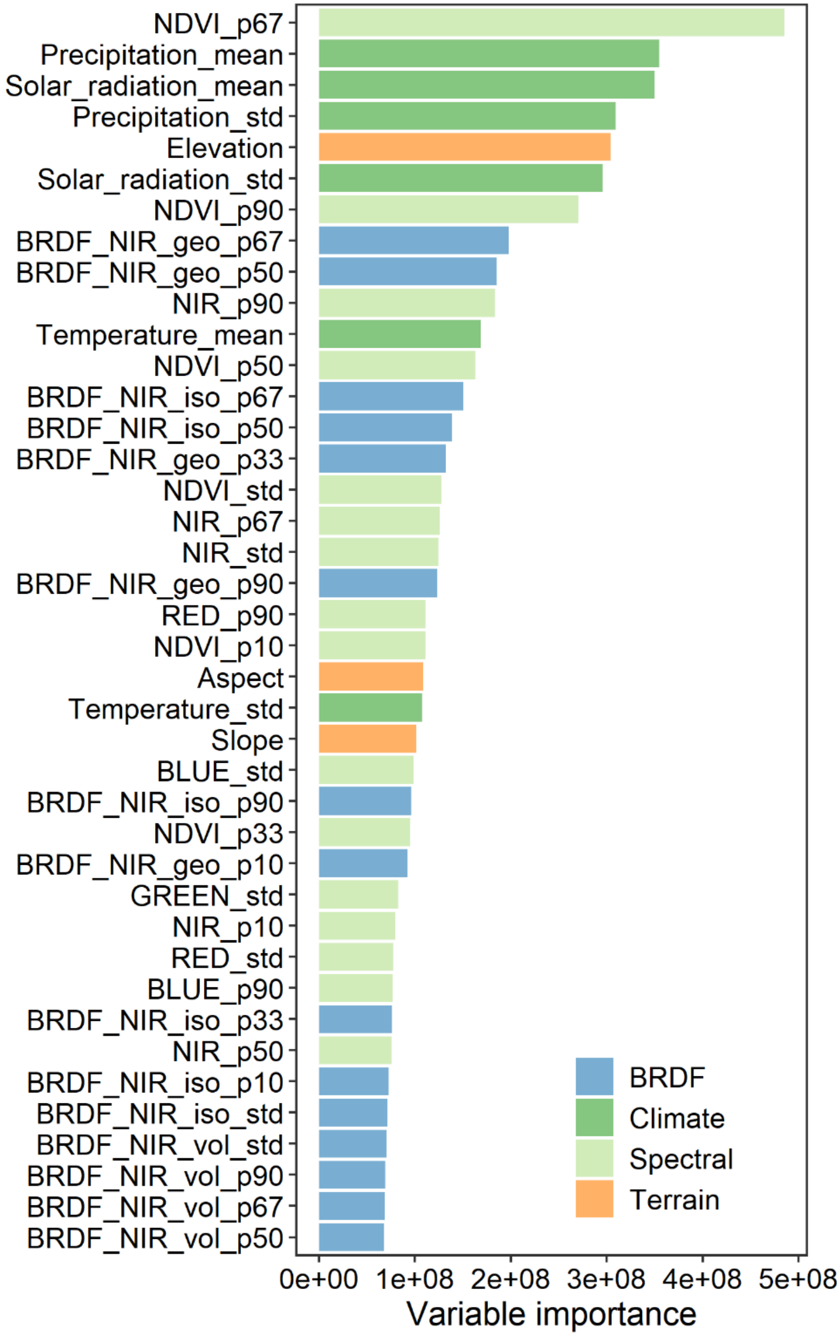

Figure 6. The importance of variables in the mean leaf inclination angle prediction. NIR, Red, Green, and Blue denote the nadir reflectance in near-infrared, red, green, and blue bands, respectively; geo, iso, and vol represent kernel coefficients of geometric-optical surface scattering, isotropic scattering, and volumetric scattering, respectively. The suffixes p××, mean, and std represent ××% quantile, mean, and standard deviation, respectively.

Fig. 7 illustrates the relationships between the upscaled MLA samples and the 16 most important variables. Overall, MLA decreases with the increase of NDVI, NIR reflectance, and NIR BRDF kernel parameters, whereas it increases with the standard deviation of NDVI. MLA is negatively correlated with solar radiation, precipitation, and temperature. Additionally, MLA increases with increasing the standard deviation of solar radiation (corresponding to mid-to-high latitude regions), while it decreases with the increase in the standard deviation of precipitation (corresponding to tropical and subtropical regions with high precipitation). MLA increases slightly with elevation.

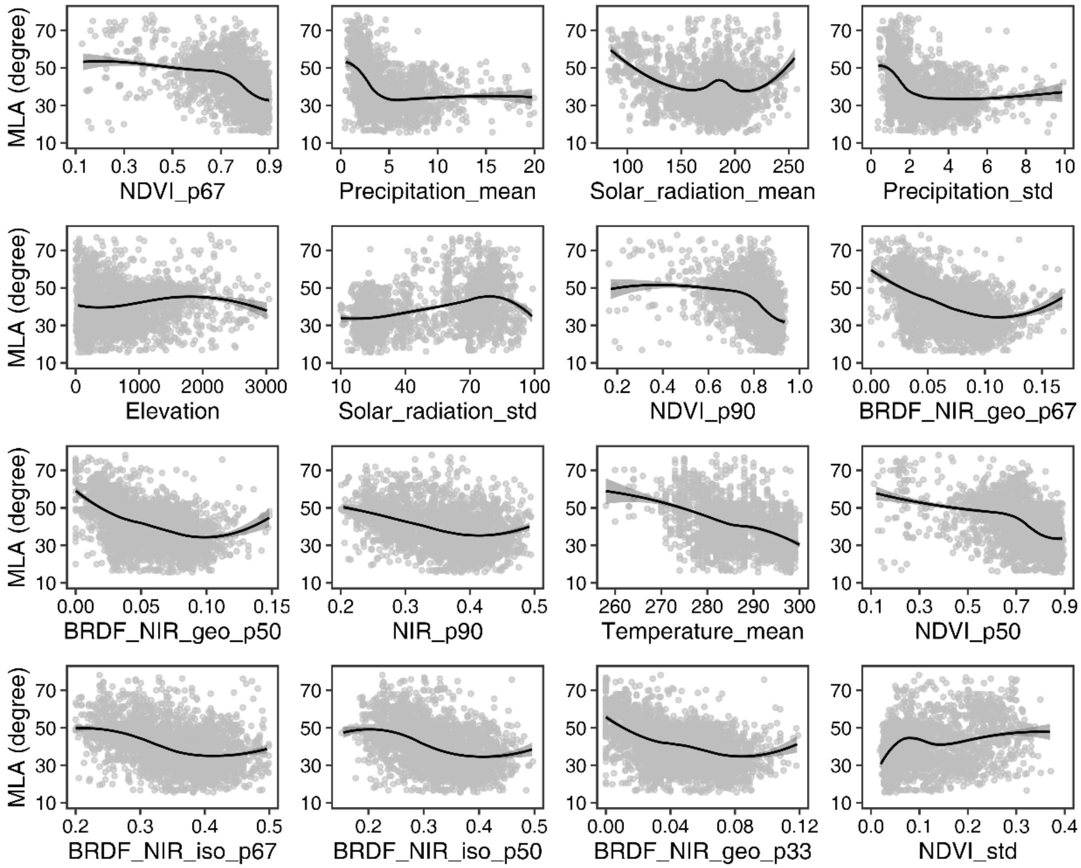

Figure 7. Relationships between mean leaf inclination angle (MLA) and different predictive variables. See Fig. 6 for different variables.

3.3 Global MLA and G(0) maps

Fig. 8 shows the spatial distribution of the global 500 m MLA product. Central Asia (grasslands), southern India (cereal crops), and the central United States (grasslands and cereal crops) show higher MLAs of approximately 60°, whereas the rainforests and Southeast Asia forests have more horizontal leaves with MLAs of around 30° (Fig. 8 and S2). MLA increases with latitude, from 32.93 ± 7.03° around the equator (~1.5° N) to 53.48 ± 3.20° in the northern tundra (~76.5° N). Variation in MLA decreases as latitude increases (Fig. 8). Among different PFTs, cereal crops show the highest MLA (54.65 ± 6.28°), while evergreen broadleaf forest has the lowest MLA (34.40 ± 6.42°), and PFTs follow the order: CRO-C > CRO-B > DNF > SHR > ENF ≈ GRA > DBF > EBF (Table 4). Grassland, broadleaf forest, and evergreen needleleaf forests show larger MLA variations than other PFTs, whereas deciduous needleleaf forests show minimal variation. The global vegetation MLA is 41.47°, with a standard deviation of 9.55°, which is comparable to the MLA of DBF (41.23 ± 6.58°) (Fig. 9a and Table 4).

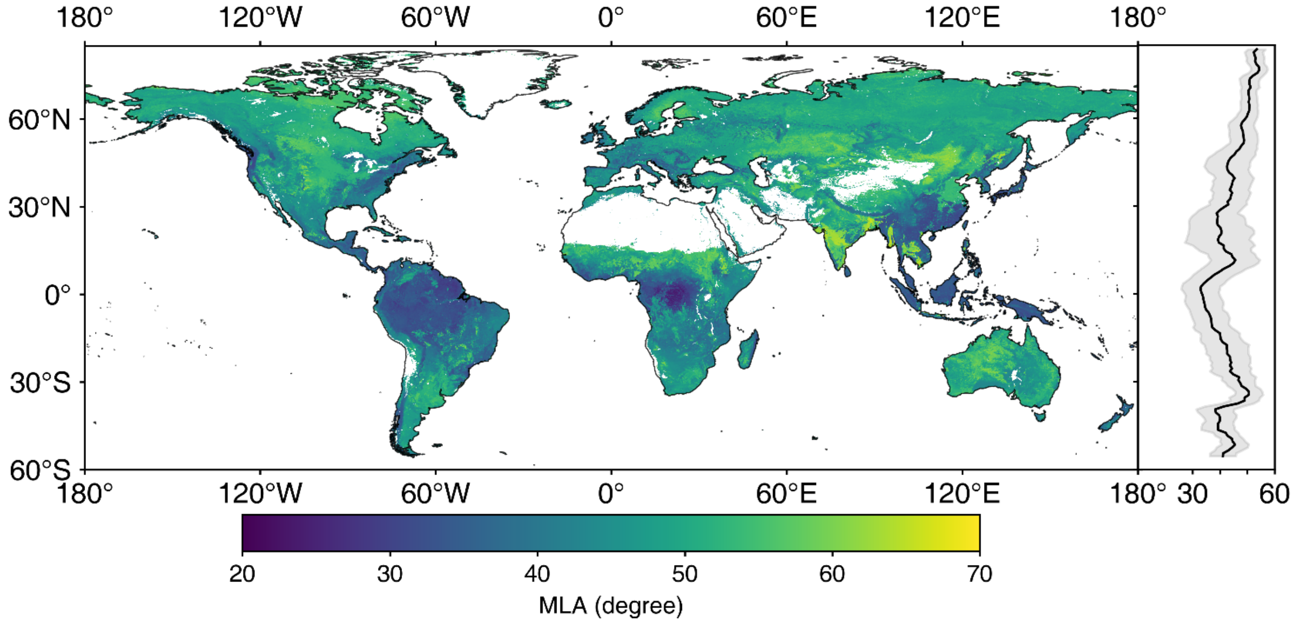

Figure 8. The global mean leaf inclination angle (MLA) map. The right panel shows the MLA latitudinal mean (solid line) and the standard deviation values (shaded area) weighted by leaf area index.

Table 4. Statistics of global mean leaf inclination angle (MLA), nadir leaf projection function (G(0)), and inclination index (χ_L) for different plant functional types (PFT). STD is the standard deviation. The χ_L is converted from MLA ($\chi_L = 2cos(\text{MLA}) - 1$) (Lawrence et al., 2019).

PFT	DBF	DNF	EBF	ENF	CRO-B	CRO-C	GRA	SHR	Globe
Area proportion(%)	14.02	6.32	15.08	11.42	2.99	6.84	28.45	14.88	100.00
MLA(°)	41.23	50.05	**34.40**	47.13	52.35	**54.65**	47.12	49.23	41.47
STD of MLA (°)	6.58	3.24	6.42	8.35	6.63	6.28	8.08	5.35	9.55
G(0)	0.69	0.58	**0.76**	0.61	0.55	**0.52**	0.61	0.59	0.68
STD of G(0)	0.07	0.03	0.06	0.08	0.07	0.08	0.09	0.06	0.11
χ_L	0.50	0.28	0.65	0.36	0.22	0.16	0.36	0.31	0.50

The global MLA exhibits an asymmetric probability density distribution toward the lower MLA (Fig. 9b). It roughly presents three peaks, with the highest peak (~51°) containing DNF, ENF, CRO, GRA, and SHR. The moderate peak (~35°) is mainly composed of EBF and DBF, while the third peak (~58°) is dominated by crops. The MLAs of crops and some grasslands are close to the MLA of the spherical distribution (57.30°). The global MLA (41.47°) is 15.83° (38%) smaller than the MLA of the spherical distribution because the vegetation MLA is mostly less than 57.30° (Fig. 9b).

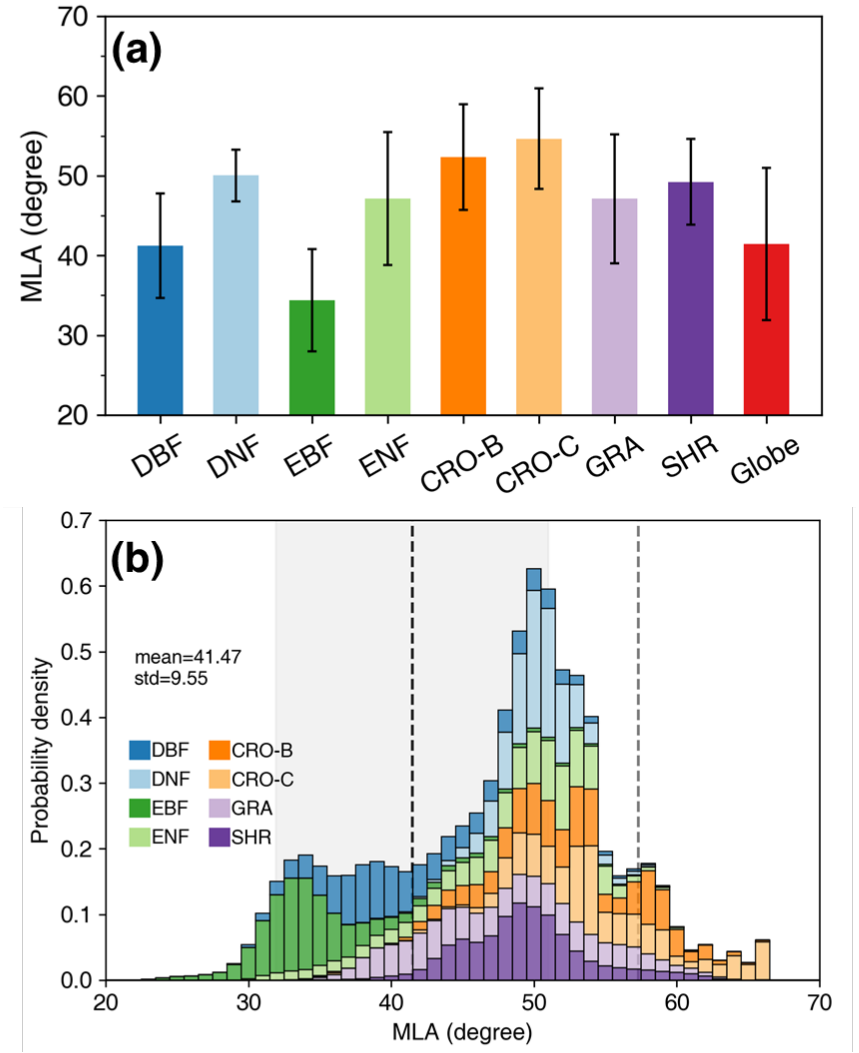

Figure 9. Statistics (a) and probability density distributions (b) of the global mean leaf inclination angle (MLA) for different plant functional types. The error bars in (a) represent the standard deviation. The black dash line and shade area in (b) indicate the global MLA mean and standard deviation. The gray dashed line represents the MLA (=57.30°) of spherical leaf angle distribution. The mean, standard deviation, and probability density values are weighted by leaf area index. See Fig. 1 for the acronyms.

Fig. 10 displays the spatial distribution of global G(0) generated from MLA. Overall, the global G(0) shows an opposite pattern with the global MLA. The G(0) values in Central Asia (grasslands, Fig. S2), southern India (cereal crops), and the central United States (grasslands and cereal crops) are relatively lower than those in tropical rainforests, forests in Southeast Asia, and forests in the eastern United States. G(0) generally decreases slowly with latitude, from 0.78 ± 0.08 at the equator (~1.5° N) to 0.52 ± 0.04 in the northern tundra (~76.5° N).

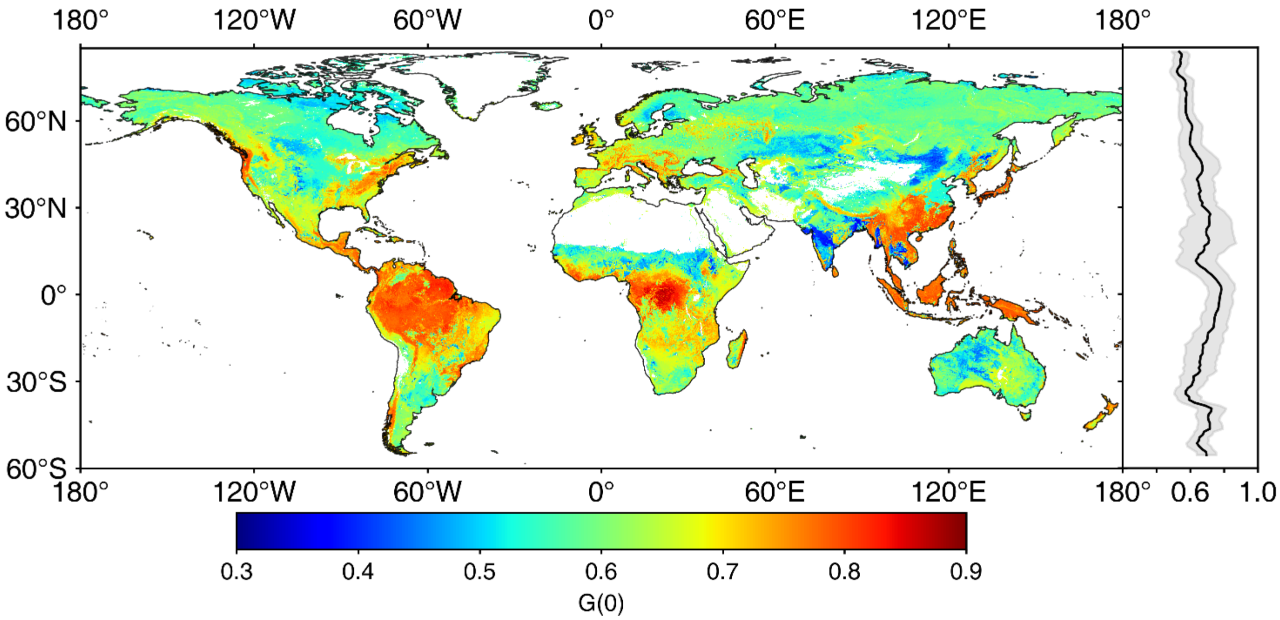

Figure 10. The global nadir leaf projection function (G(0)) map. The right panel shows the G(0) mean (solid line) and standard deviation values (shaded area) weighted by leaf area index.

Among different PFTs, EBF has the highest G(0), at approximately 0.76 ± 0.06 (Fig. 11a, Table 4), whereas cereal crops show the lowest value, at approximately 0.52 ± 0.08. The DBF G(0) is comparable to the global average. The G(0) of broad-leaved forests is greater than that of other PFTs (Fig. 11a, Table 4). The global G(0) probability density distribution peaks at 0.52–0.65, with an asymmetric distribution (Fig. 11b). The proportion on the right side of the peak is larger than that on the left. The peak of the global G(0) distribution mainly contains DNF, ENF, CRO, GRA, and SHR. The left side of the peak is mainly composed of crops, while the right side is dominated by broad-leaved forests and some shrubs. The spherical distribution G(0) (0.50) is mainly represented by crops and a small amount of grassland, where G(0) also shows a large variation (~0.35). The spherical distribution G(0) is 0.18 (26%) less than the global average G(0) (0.68), as most vegetation G(0) is greater than 0.50 (Fig. 11b).

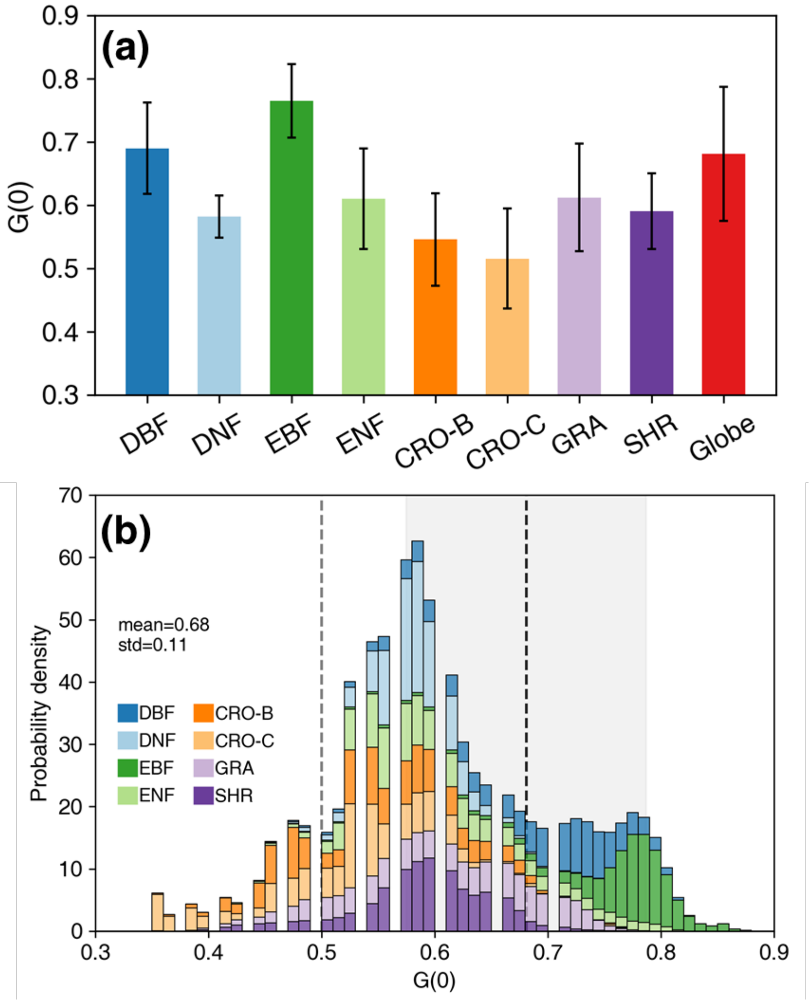

Figure 11. Statistics (a) and probability density distributions (b) of the global nadir leaf projection function (G(0)) for different plant functional types. The error bars in (a) represent the standard deviation. The black dash line and shade area in (b) indicate the global G(0) mean and standard deviation. The gray dashed line represents the G(0) (=0.50) of spherical leaf angle distribution. The mean, standard deviation, and probability density values are weighted by leaf area index. See Fig. 1 for the acronyms.

3.4 Evaluation of global MLA

Fig. 12 shows the comparison between the predicted MLA and upscaled MLA samples using the ten-fold cross-validation method. For noncrops, the predicted MLA is moderately consistent with the upscaled sample MLA (r = 0.75, RMSE = 7.15°), with 83% of samples having residuals < 10° and 94% of samples having residuals < 15°. For DNF and SHR, the predicted MLA compresses the variation range of sample MLA (Fig. 12a). For crops, the predicted MLA of CRO-C shows higher consistency (r = 0.60) than that of CRO-B (r = 0.48). (Fig. 12b and c).

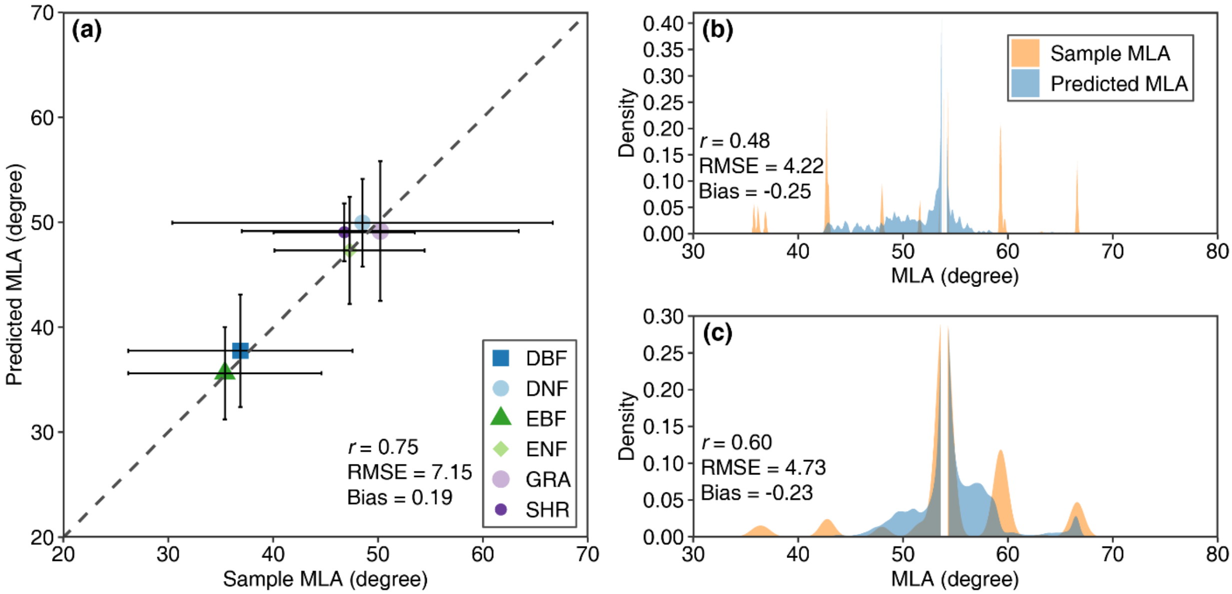

Figure 12. Comparisons between predicted MLA and sample MLA for noncrop (a), broadleaf crops (b), and cereal crops (c) (See Fig. 1 for the acronyms). The error bar in (a) represents the standard deviation.

Fig. 13 compares G(0) derived from the MLA and high-resolution reference data. The MLA-derived G(0) shows moderate consistency with the reference G(0) ($r = 0.62$), and 65% of the estimated G(0) residuals are < 0.15, and 84% of the residuals are < 0.20. The estimated G(0) generally overestimates (bias = 0.11), especially when G(0) is low (< 0.60), mainly for crops, pasture, woody wetlands, and shrubs, whereas grasslands show better consistency. The estimated G(0) is temporally more stable than the reference G(0) which is generally greater than 0.50 and displays seasonal variation (horizontally distributed bars in Fig. 13).

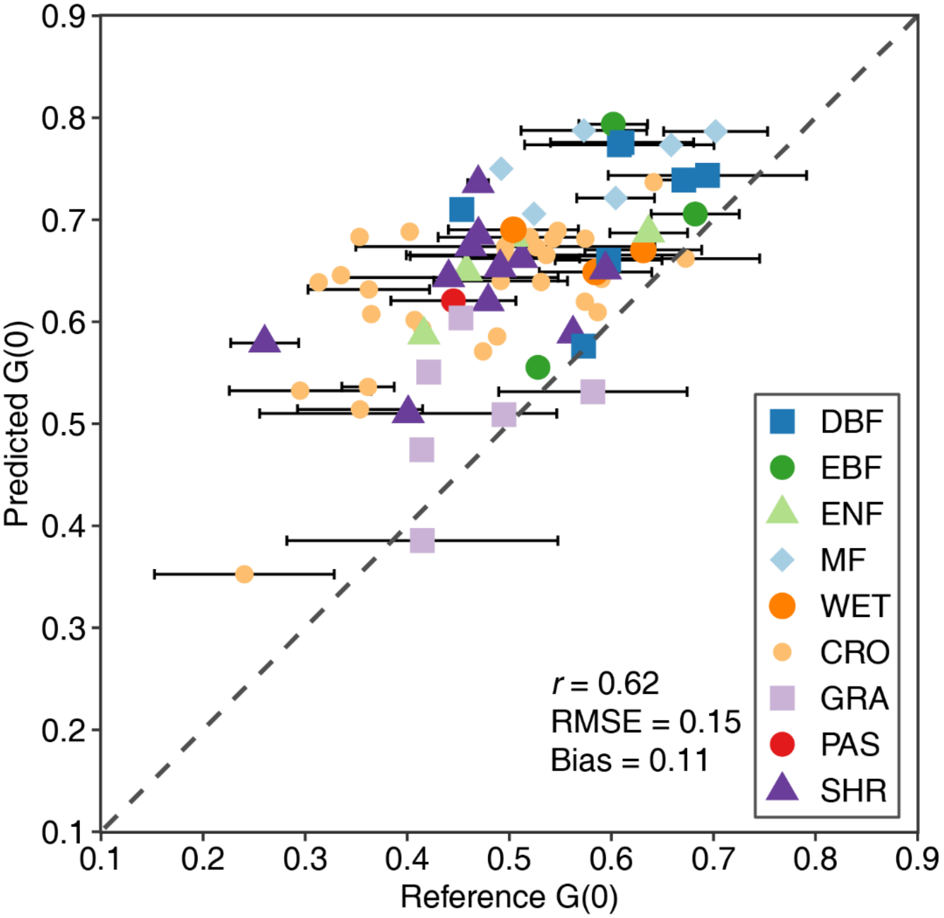

Figure 13. Comparisons of G(0) derived from mean leaf inclination angle and high-resolution reference data for different plant functional types (see Fig. 2 for the acronyms). The error bar represents the standard deviation of reference G(0) at different seasons.

4 Discussion

4.1 Global MLA and G(0)

This study compiled global LIA field measurements and generated the first global 500 m MLA and G(0) maps (Figs. 8 and 10). These maps show the average MLA and G(0) conditions during the growing seasons from 2001 to 2022. Overall, the global MLA is lowest around the equator and increases with latitude (Figs. 8 and 10). This accords with the MLA latitude variation derived from model simulations (Huemmrich, 2013). Crops have higher MLA than broadleaf forests whose leaves are relatively horizontal. The global MLA and G(0) maps enhance our understanding of the global distribution of MLA and G(0) and should be useful in radiative transfer modeling, remote sensing of vegetation parameters, land surface modeling, and ecological studies.

The globally derived MLA is 41.47°, which is consistent with the LIA measurements (40.74°, Tables 3 and 4). However, the derived MLAs of DBF, DNF, CRO-B, and SHR are approximately 10° greater than the measured MLAs. It is noted that the number and spatial distribution of LIA measurements for these biomes are limited. For example, the global CRO-B areas are dominated by soybeans with higher LIA (Table S2), and the LIA measurements for soybeans are limited, which caused the CRO-B MLA in the global map to be greater than that in the measurement statistics (Tables 3 and 4). The poor crop MLA prediction (Fig. 12b) is mainly caused by a small number of samples and the strong seasonal variation. It is difficult to consider within-crop LIA variation when typical MLA values are assigned to different crops.

Due to the lack of high-resolution reference MLA, the global MLA was evaluated through a comparison of the MLA-derived G(0) with the high-resolution reference G(0) (Fig. 13). The result shows medium consistency but MLA-derived G(0) overestimates at low values (< 0.60), especially for CRO, PAS, SHR, and WET. The overestimation may be partly caused by the underestimation of MLA at high values that is related to the errors introduced in the sample expansion and upscaling. These errors are mainly caused by a lack of LIA measurements, vegetation structural complexity, and seasonal variation. In addition, the uncertainties in the reference G(0) may have contributed to the overestimation. The reference G(0) was derived from the Beer-Lambert law (Eq. (4)) which assumes that the canopy is a turbid medium. The turbid medium assumption is unrealistic for complex vegetation (Widlowski et al., 2014). The angular variation of CI and the mixture of branches and leaves in generating high-resolution G(0) can also lead to the overestimation. Previous studies have shown that CI increases with the view zenith angle (Fang, 2021), which means that the whole CI > CI(0) and can lead to the underestimation of the reference G(0) (Eq. (6) and (7)). The mixture of branches and leaves may result in the underestimation of the reference G(0) due to the usually higher inclination angle of the trunks (Liu et al., 2019). Compared with the previous G(0) derived from global vegetation biophysical products (Eq. (7)) ($R^2 = 0.11$, RMSE = 0.53) (Li et al., 2022), the MLA-derived G(0) performs better ($R^2 = 0.38$, RMSE = 0.15).

In addition, the G(0) data obtained from our study can be used to derive the G(θ) for any arbitrary angle. One method of getting G(θ) is based on single-parameter ellipsoidal leaf angle distribution (Campbell, 1990) (Eq. (3)). Another method is to make use of both G(0) and G(57.3°) (≡ 0.5) and derive G(θ) using a simple linear ($G(\theta) = a \cdot \theta + b$) or sinusoidal ($G(\theta) = a \cdot sin(\theta) + b$)) interpolation method. Since G(θ) varies most significantly in the nadir direction for different MLA (Wilson, 1959), the uncertainty of G(θ) derived from the global MLA in other directions will be smaller than that of G(0).

4.2 The relationship between MLA and other variables

Analysis of the relationships between MLA and other features in the MLA mapping process reveals that MLA is negatively correlated with NDVI, NIR reflectance, and NIR BRDF kernel coefficients (Fig. 7). These findings are consistent with other simulation and experimental studies (Zou and Mõttus, 2015; Liu et al., 2012; Dong et al., 2019; Jacquemoud et al., 1994). Higher LIA means lower radiation interception, more NIR downward radiation, and lower NIR reflectance (Liu et al., 2012).

This results in negative correlations between MLA and NIR reflectance and vegetation index. The negative relationships between MLA and radiation, precipitation, and temperature (Fig. 7) are related to the vegetation adaptation mechanism. Under suitable climate conditions, horizontal leaves make better usage of precipitation radiation, precipitation, and temperature and increase the photosynthesis rate (Van Zanten et al., 2010; King, 1997). The positive correlation between MLA and the standard deviation of radiation and temperature (Fig. 7) indicates that the MLA is more vertical in areas with significant seasonal changes in radiation and temperature (mid to high-latitude areas) because vertical leaves maximize intercepted radiation under low solar altitudes at mid to high-latitude areas (Huemmrich, 2013).

4.3 Use of the new MLA map

The spherical LAD assumption has been widely adopted in the literature (Tang et al., 2016; Zhao et al., 2020; Wang and Fang, 2020). This study demonstrates that the spherical assumption is valid only for cereal crops, but not for broadleaf forests (Tables 3 and 4). This finding is consistent with previous local LIA measurements (De Wit, 1965; Pisek et al., 2013; Yan et al., 2021). For crops, the spherical assumption may even become invalid because of seasonality and species diversity (Table S2, Figs. 5 and 9). Fig. 13 shows that most of the reference G(0) values are greater than 0.50, while the spherical distribution would underestimate the interception of radiation and rainfall (Figs. 9 and 11) (Stadt and Lieffers, 2000). In current LSMs, a constant LIA is commonly assigned for each PFT (Majasalmi and Bright, 2019). For example, the Community Land Model V5 (CLM5) (Table S4) (Lawrence et al., 2019) uses lower inclination indices and higher LIA values than our results (Tables 3 and 4) and thus may underestimate canopy interception. The global LIA map generated in this study provides a more reasonable LIA parameterization strategy for the application communities.

4.4 Limitations and prospects

The limitations of this study relate to the small number of LIA measurements, especially continuous measurements. First, within-species LIA variations were neglected in the spatial expansion due to limited spatial coverage of existing LIA-measured data (Section 2.3.1). This may introduce some errors, especially for crops. Second, the LIA measurement data were obtained using different sampling schemes and methods. This inconsistency may influence the results. Third, for forests, the contribution of the understory was not considered. Typically, the understory is characterized by more horizontal leaves, and ignoring the understory may lead to an MLA overestimation (Utsugi et al., 2006). Nevertheless, a previous study showed that the relative contribution of the understory to the overall MLA is less than 10% (Li et al., 2022). Finally, only the growing season MLA was calculated, whereas the seasonal and long-term variations of MLA were not considered due to the lack of continuous LIA measurements.

In the future, more efficient LIA observation systems should be developed to provide continuous LIA data (Kattenborn et al., 2022). LIA measurements can be integrated into existing ground observation networks, such as the National Ecological Observatory Network (NEON) (Kao et al., 2012), Integrated Carbon Observation System (ICOS) (Gielen et al., 2018), and Terrestrial Ecosystem Research Network (TERN) (Karan et al., 2016), to enhance temporal LIA measurements in larger spatial extent, especially for DNF and crops. The formulation of standard measurement and data-sharing protocols will promote data-sharing and utilization (Li et al., 2023). Multiangle reflectance (Jacquemoud et al., 2009; Goel and Thompson, 1984; Jacquemoud et al., 1994) or light detection and ranging (Zheng and Moskal, 2012; Bailey and Mahaffee, 2017; Itakura and Hosoi, 2019) are encouraging remote sensing tools that can help to derive temporally continuous and high-resolution MLA data.

5 Conclusion

This study compiled existing global LIA measurements and generated the first global 500 m MLA and G(0) products by gap-filling the LIA measurement data using a random forest regressor. The mean of global LIA measurements is 40.74° and cereal crops show the highest MLA (59.11°). The global MLA shows an explicit spatial distribution and the value increases with latitude. The global MLA is 41.47° ± 9.55° and follows the order of CRO-C > CRO-B > DNF > SHR > ENF ≈ GRA > DBF > EBF. The predicted MLA presents a medium consistency (r = 0.75, RMSE = 7.15°) with the validation samples for noncrops. For crops, the results are relatively poorer (r = 0.48 and 0.60 for broadleaf crops and cereal crops) because of limited LIA measurements and strong seasonality. The G(0) derived from MLA is moderately consistent with the reference G(0) (r = 0.62).

The MLA and G(0) products obtained in this study would enhance our understanding of global LIA and assist remote sensing retrieval and land surface modeling studies. These products provide a more realistic parameterization strategy than the commonly used spherical LAD and PFT-specific MLA assignment. Note the global MLA and G(0) products mainly represent the typical state during the growing season. These products can be further improved and temporal MLA data can be obtained through continuous measurements and remote sensing retrieval.

Data availability

The global MLA and G(0) products are available in: Li, S. and Fang, H. 2024, https://doi.org/10.5281/zenodo.10940673. (Li and Fang, 2024). The related code can be accessed at https://code.earthengine.google.com/?accept_repo=users/SiJia/MTA.

Author contributions

HF and SL conceptualized this work. SL compiled global LIA measurements, generated global products, and curated the datasets. SL and HF wrote the manuscript. HF was responsible for funding and supervision.

Competing interests

The contact author has declared that none of the authors has any competing interests.

Acknowledgements

The authors are grateful to TRY and many other researchers for sharing the LIA measurement data. Jens Kattge at the Max Planck Institute for Biogeochemistry and Dongliang Cheng at Fujian Normal University provided the TRY species location data and LIA measurements in China's subtropical regions, respectively.

Financial support

This work was mainly supported by the National Natural Science Foundation of China (42171358).

References

Alexandridis, T. K., Ovakoglou, G., and Clevers, J. G. P. W.: Relationship between MODIS EVI and LAI across time and space, Geocarto International, 35, 1385-1399, 10.1080/10106049.2019.1573928, 2019.

Bailey, B. N. and Mahaffee, W. F.: Rapid measurement of the three-dimensional distribution of leaf orientation and the leaf angle probability density function using terrestrial LiDAR scanning, Remote Sens. Environ., 194, 63-76, 10.1016/j.rse.2017.03.011, 2017.

Bayat, B., van der Tol, C., and Verhoef, W.: Integrating satellite optical and thermal infrared observations for improving daily ecosystem functioning estimations during a drought episode, Remote Sens. Environ., 209, 375-394, 10.1016/j.rse.2018.02.027, 2018.

Boryan, C., Yang, Z., Mueller, R., and Craig, M.: Monitoring US agriculture: the US department of agriculture, national agricultural statistics service, cropland data layer program, Geocarto International, 26, 341-358, 2011.

Brown, L. A., Meier, C., Morris, H., Pastor-Guzman, J., Bai, G., Lerebourg, C., Gobron, N., Lanconelli, C., Clerici, M., and Dash, J.: Evaluation of global leaf area index and fraction of absorbed photosynthetically active radiation products over North America using Copernicus Ground Based Observations for Validation data, Remote Sens. Environ., 247, 10.1016/j.rse.2020.111935, 2020.

Campbell, G.: Derivation of an angle density function for canopies with ellipsoidal leaf angle distributions, Agricultural and forest meteorology, 49, 173-176, 1990.

Chen, J. M., Ju, W., Ciais, P., Viovy, N., Liu, R., Liu, Y., and Lu, X.: Vegetation structural change since 1981 significantly enhanced the terrestrial carbon sink, Nat Commun, 10, 4259, 10.1038/s41467-019-12257-8, 2019.

Chen, X., Zhong, Q.-L., Lyu, M., Wang, M., Hu, D., Sun, J., and Cheng, D.: Trade-off relationship between light interception and leaf water shedding at different canopy positions of 73 broad-leaved trees of Yangji Mountain in Jiangxi Province, China, SCIENTIA SINICA Vitae, 51, 91-101, 10.1360/SSV-2020-0218, 2021.

Chianucci, F., Pisek, J., Raabe, K., Marchino, L., Ferrara, C., and Corona, P.: A dataset of leaf inclination angles for temperate and boreal broadleaf woody species, Annals of Forest Science, 75, 50-50, 10.1007/s13595-018-0730-x, 2018.

Crawford, C. J., Roy, D. P., Arab, S., Barnes, C., Vermote, E., Hulley, G., Gerace, A., Choate, M., Engebretson, C., Micijevic, E., Schmidt, G., Anderson, C., Anderson, M., Bouchard, M., Cook, B., Dittmeier, R., Howard, D., Jenkerson, C., Kim, M., Kleyians, T., Maiersperger, T., Mueller, C., Neigh, C., Owen, L., Page, B., Pahlevan, N., Rengarajan, R., Roger, J.-C., Sayler, K., Scaramuzza, P., Skakun, S., Yan, L., Zhang, H. K., Zhu, Z., and Zahn, S.: The 50-year Landsat collection 2 archive, Science of Remote Sensing, 8, 100103, https://doi.org/10.1016/j.srs.2023.100103, 2023.

d'Andrimont, R., Verhegghen, A., Lemoine, G., Kempeneers, P., Meroni, M., and van der Velde, M.: From parcel to continental scale – A first European crop type map based on Sentinel-1 and LUCAS Copernicus in-situ observations, Remote Sens. Environ., 266, 112708, https://doi.org/10.1016/j.rse.2021.112708, 2021.

de Wit, C. T.: Photosynthesis of leaf canopies, Pudoc, 1965.

Dong, J., fu, y., wang, j., Tian, H., Fu, S., Niu, Z., Han, W., Zheng, Y., Huang, J., and Yuan, W.: 30m winter wheat distribution map of China for four years (2016-2019), 10.6084/m9.figshare.12003990.v2, 2020.

Dong, T., Liu, J., Shang, J., Qian, B., Ma, B., Kovacs, J. M., Walters, D., Jiao, X., Geng, X., and Shi, Y.: Assessment of red-edge vegetation indices for crop leaf area index estimation, Remote Sens. Environ., 222, 133-143, 10.1016/j.rse.2018.12.032, 2019.

Fang, H.: Canopy clumping index (CI): A review of methods, characteristics, and applications, Agricultural and Forest Meteorology, 303, 108374, https://doi.org/10.1016/j.agrformet.2021.108374, 2021.

Fang, H., Li, S., Zhang, Y., Wei, S., and Wang, Y.: New insights of global vegetation structural properties through an analysis of canopy clumping index, fractional vegetation cover, and leaf area index, Science of Remote Sensing, 100027, https://doi.org/10.1016/j.srs.2021.100027, 2021.

Fisette, T., Rollin, P., Aly, Z., Campbell, L., Daneshfar, B., Filyer, P., Smith, A., Davidson, A., Shang, J., and Jarvis, I.: AAFC annual crop inventory, 2013 Second International Conference on Agro-Geoinformatics (Agro-Geoinformatics), 270-274,

Foley, J. A., Prentice, I. C., Ramankutty, N., Levis, S., Pollard, D., Sitch, S., and Haxeltine, A.: An integrated biosphere model of land surface processes, terrestrial carbon balance, and vegetation dynamics, Global biogeochemical cycles, 10, 603-628, 1996.

Gielen, B., Acosta, M., Altimir, N., Buchmann, N., Cescatti, A., Ceschia, E., Fleck, S., Hörtnagl, L., Klumpp, K., Kolari, P., Lohila, A., Loustau, D., Marańon-Jimenez, S., Manise, T., Matteucci, G., Merbold, L., Metzger, C., Moureaux, C., Montagnani, L., Nilsson, M. B., Osborne, B., Papale, D., Pavelka, M., Saunders, M., Simioni, G., Soudani, K., Sonnentag, O., Tallec, T., Tuittila, E.-S., Peichl, M., Pokorny, R., Vincke, C., and Wohlfahrt, G.: Ancillary vegetation measurements at ICOS ecosystem stations, International Agrophysics, 32, 645-664, 10.1515/intag-2017-0048, 2018.

Goel, N. S. and Thompson, R. L.: Inversion of vegetation canopy reflectance models for estimating agronomic variables. V. Estimation of leaf area index and average leaf angle using measured canopy reflectances, Remote Sens. Environ., 16, 69-85, 10.1016/0034-4257(84)90028-2, 1984.

Han, J., Zhang, Z., Luo, Y., Cao, J., Zhang, L., Cheng, F., Zhuang, H., Zhang, J., and Tao, F.: NESEA-Rice10: high-resolution annual paddy rice maps for Northeast and Southeast Asia from 2017 to 2019, Earth System Science Data, 13, 5969-5986, 10.5194/essd-13-5969-2021, 2021.

Hinojo-Hinojo, C. and Goulden, M.: A compilation of canopy leaf inclination angle measurements across plant species and biome types, 10.7280/D1T97H, 2020.

Huemmrich, K. F.: Simulations of Seasonal and Latitudinal Variations in Leaf Inclination Angle Distribution: Implications for Remote Sensing, Advances in Remote Sensing, 02, 93-101, 10.4236/ars.2013.22013, 2013.

Itakura, K. and Hosoi, F.: Estimation of Leaf Inclination Angle in Three-Dimensional Plant Images Obtained from Lidar, Remote Sensing, 11, 10.3390/rs11030344, 2019.

Jacquemoud, S., Flasse, S., Verdebout, J., and Schmuck, G.: Comparison of Several Optimization Methods To Extract Canopy Biophysical Parameters - Application To Caesar Data, 291-298, 1994.

Jacquemoud, S., Verhoef, W., Baret, F., Bacour, C., Zarco-Tejada, P. J., Asner, G. P., François, C., and Ustin, S. L.: PROSPECT+SAIL models: A review of use for vegetation characterization, Remote Sens. Environ., 113, S56-S66, 10.1016/j.rse.2008.01.026, 2009.

Kao, R. H., Gibson, C. M., Gallery, R. E., Meier, C. L., Barnett, D. T., Docherty, K. M., Blevins, K. K., Travers, P. D., Azuaje, E., Springer, Y. P., Thibault, K. M., McKenzie, V. J., Keller, M., Alves, L. F., Hinckley, E.-L. S., Parnell, J., and Schimel, D.: NEON terrestrial field observations: designing continental-scale, standardized sampling, Ecosphere, 3, art115, 10.1890/es12-00196.1, 2012.

Karan, M., Liddell, M., Prober, S. M., Arndt, S., Beringer, J., Boer, M., Cleverly, J., Eamus, D., Grace, P., Van Gorsel, E., Hero, J. M., Hutley, L., Macfarlane, C., Metcalfe, D., Meyer, W., Pendall, E., Sebastian, A., and Wardlaw, T.: The Australian SuperSite Network: A continental, long-term terrestrial ecosystem observatory, Sci. Total Environ., 568, 1263-1274, 10.1016/j.scitotenv.2016.05.170, 2016.

Kattenborn, T., Richter, R., Guimarães-Steinicke, C., Feilhauer, H., and Wirth, C.: AngleCam: Predicting the temporal variation of leaf angle distributions from image series with deep learning, Methods in Ecology and Evolution, 13, 2531-2545, 10.1111/2041-210x.13968, 2022.

Kattge, J., Bonisch, G., Diaz, S., Lavorel, S., and Prentice, I. C.: TRY plant trait database - enhanced coverage and open access, Glob Chang Biol, 26, 119-188, 10.1111/gcb.14904, 2020.

King, D. A.: The Functional Significance of Leaf Angle in Eucalyptus, Aust. J. Bot., 45, 619-639, https://doi.org/10.1071/BT96063, 1997.

Kuusk, A.: A two-layer canopy reflectance model, Journal of Quantitative Spectroscopy and Radiative Transfer, 71, 1-9, https://doi.org/10.1016/S0022-4073(01)00007-3, 2001.

Lang, A. R. G.: Leaf orientation of a cotton plant, Agricultural Meteorology, 11, 37-51, 10.1016/0002-1571(73)90049-6, 1973.

Lawrence, D. M., Fisher, R. A., Koven, C. D., Oleson, K. W., Swenson, S. C., Bonan, G., Collier, N., Ghimire, B., Van Kampenhout, L., and Kennedy, D.: The Community Land Model version 5: Description of new features, benchmarking, and impact of forcing uncertainty, Journal of Advances in Modeling Earth Systems, 11, 4245-4287, 2019.

Li, S. and Fang, H.: Global Leaf Inclination Angle (LIA) and Nadir Leaf Projection Function (G(0)) Products, Zenodo [dataset], 10.5281/zenodo.10940673, 2024.

Li, S., Fang, H., and Zhang, Y.: Determination of the Leaf Inclination Angle (LIA) through Field and Remote Sensing Methods: Current Status and Future Prospects, Remote Sensing, 15, 946, 2023.

Li, S., Fang, H., Zhang, Y., and Wang, Y.: Comprehensive evaluation of global CI, FVC, and LAI products and their relationships using high-resolution reference data, Science of Remote Sensing, 6, 10.1016/j.srs.2022.100066, 2022.

Liu, J., Pattey, E., and Jégo, G.: Assessment of vegetation indices for regional crop green LAI estimation from Landsat images over multiple growing seasons, Remote Sens. Environ., 123, 347-358, 10.1016/j.rse.2012.04.002, 2012.

Liu, J., Wang, T., Skidmore, A. K., Jones, S., Heurich, M., Beudert, B., and Premier, J.: Comparison of terrestrial LiDAR and digital hemispherical photography for estimating leaf angle distribution in European broadleaf beech forests, ISPRS Journal of Photogrammetry and Remote Sensing, 158, 76-89, 10.1016/j.isprsjprs.2019.09.015, 2019.

Maes, W. and Steppe, K.: Estimating evapotranspiration and drought stress with ground-based thermal remote sensing in agriculture: a review, J. Exp. Bot., 63, 4671-4712, 2012.

Majasalmi, T. and Bright, R. M.: Evaluation of leaf-level optical properties employed in land surface models – example with CLM 5.0, Geoscientific Model Development Discussions, 1-24, 2019.

Mantilla-Perez, M. B. and Salas Fernandez, M. G.: Differential manipulation of leaf angle throughout the canopy: current status and prospects, J. Exp. Bot., 68, 5699-5717, 2017.

Muñoz-Sabater, J., Dutra, E., Agustí-Panareda, A., Albergel, C., Arduini, G., Balsamo, G., Boussetta, S., Choulga, M., Harrigan, S., Hersbach, H., Martens, B., Miralles, D. G., Piles, M., Rodríguez-Fernández, N. J., Zsoter, E., Buontempo, C., and Thépaut, J.-N.: ERA5-Land: a state-of-the-art global reanalysis dataset for land applications, Earth System Science Data, 13, 4349-4383, 10.5194/essd-13-4349-2021, 2021.

Myneni, R., Knyazikhin, Y., Park, T.: MCD15A2H MODIS/Terra+Aqua Leaf Area Index/FPAR 8-day L4 Global 500m SIN Grid V006 [dataset], http://doi.org/10.5067/MODIS/MCD15A2H.006, 2015.

Nilson, T.: A theoretical analysis of the frequency of gaps in plant stands, Agricultural Meteorology, 8, 25-38, 1971.

Norman, J. M. and Campbell, G. S.: Canopy structure, in: Plant Physiological Ecology: Field methods and instrumentation, edited by: Pearcy, R. W., Ehleringer, J. R., Mooney, H. A., and Rundel, P. W., Springer Netherlands, Dordrecht, 301-325, 10.1007/978-94-009-2221-1_14, 1989.

Pisek, J. and Adamson, K.: Dataset of leaf inclination angles for 71 different Eucalyptus species, Data Brief, 33, 106391, 10.1016/j.dib.2020.106391, 2020.

Pisek, J., Ryu, Y., and Alikas, K.: Estimating leaf inclination and G-function from leveled digital camera photography in broadleaf canopies, Trees, 25, 919-924, 10.1007/s00468-011-0566-6, 2011.

Pisek, J., Sonnentag, O., Richardson, A. D., and Mõttus, M.: Is the spherical leaf inclination angle distribution a valid assumption for temperate and boreal broadleaf tree species?, Agricultural and Forest Meteorology, 169, 186-194, 10.1016/j.agrformet.2012.10.011, 2013.

Pisek, J., Diaz-Pines, E., Matteucci, G., Noe, S., and Rebmann, C.: On the leaf inclination angle distribution as a plant trait for the most abundant broadleaf tree species in Europe, Agricultural and Forest Meteorology, 323, 10.1016/j.agrformet.2022.109030, 2022.

Raabe, K., Pisek, J., Sonnentag, O., and Annuk, K.: Variations of leaf inclination angle distribution with height over the growing season and light exposure for eight broadleaf tree species, Agricultural and Forest Meteorology, 214-215, 2-11, 10.1016/j.agrformet.2015.07.008, 2015.

Ross, J.: Radiative transfer in plant communities, Vegetation and the Atmosphere, 13-55, 1975.

Ross, J.: The radiation regime and architecture of plant stands, 3, Springer Science & Business Media1981.

Ryu, Y., Sonnentag, O., Nilson, T., Vargas, R., Kobayashi, H., Wenk, R., and Baldocchi, D. D.: How to quantify tree leaf area index in an open savanna ecosystem: A multi-instrument and multi-model approach, Agricultural and Forest Meteorology, 150, 63-76, 10.1016/j.agrformet.2009.08.007, 2010.

Schaaf, C. and Wang, Z.: MCD43A1 MODIS/Terra+Aqua BRDF/Albedo Model Parameters Daily L3 Global - 500m V006, NASA EOSDIS Land Processes Distributed Active Archive Center [dataset], https://doi.org/10.5067/MODIS/MCD43A1.006, 2015a.

Schaaf, C. and Wang, Z.: MCD43A4 MODIS/Terra+Aqua BRDF/Albedo Nadir BRDF Adjusted Ref Daily L3 Global - 500m V006, NASA EOSDIS Land Processes Distributed Active Archive Center [dataset], https://doi.org/10.5067/MODIS/MCD43A4.006, 2015b.

Sellers, P. J.: Canopy reflectance, photosynthesis and transpiration, International Journal of Remote Sensing, 6, 1335-1372, 10.1080/01431168508948283, 1985.

Shen, R., Dong, J., Yuan, W., Han, W., Ye, T., and Zhao, W.: A 30-m Resolution Distribution Map of Maize for China Based on Landsat and Sentinel Images, Journal of Remote Sensing, 2022, doi:10.34133/2022/9846712, 2022.

Stadt, K. J. and Lieffers, V. J.: MIXLIGHT: a flexible light transmission model for mixed-species forest stands, Agricultural and Forest Meteorology, 102, 235-252, 2000.

Sulla-Menashe, D., Gray, J. M., Abercrombie, S. P., and Friedl, M. A.: Hierarchical mapping of annual global land cover 2001 to present: The MODIS Collection 6 Land Cover product, Remote Sens. Environ., 222, 183-194, 10.1016/j.rse.2018.12.013, 2019.

Tadono, T., Ishida, H., Oda, F., Naito, S., Minakawa, K., and Iwamoto, H.: Precise global DEM generation by ALOS PRISM, ISPRS Annals of the Photogrammetry, Remote Sensing and Spatial Information Sciences, 2, 71-76, 2014.

Tang, H., Ganguly, S., Zhang, G., Hofton, M. A., Nelson, R. F., and Dubayah, R.: Characterizing leaf area index (LAI) and vertical foliage profile (VFP) over the United States, Biogeosciences, 13, 239-252, 10.5194/bg-13-239-2016, 2016.

Toda, M., Ishihara, M. I., Doi, K., and Hara, T.: Determination of species-specific leaf angle distribution and plant area index in a cool-temperate mixed forest from UAV and upward-pointing digital photography, Agricultural and Forest Meteorology, 325, 10.1016/j.agrformet.2022.109151, 2022.

Utsugi, H., Araki, M., Kawasaki, T., and Ishizuka, M.: Vertical distributions of leaf area and inclination angle, and their relationship in a 46-year-old Chamaecyparis obtusa stand, For. Ecol. Manage., 225, 104-112, https://doi.org/10.1016/j.foreco.2005.12.028, 2006.

van Zanten, M., Pons, T. L., Janssen, J. A. M., Voesenek, L. A. C. J., and Peeters, A. J. M.: On the Relevance and Control of Leaf Angle, Crit. Rev. Plant Sci., 29, 300-316, 10.1080/07352689.2010.502086, 2010.

Verhoef, W., Jia, L., Xiao, Q., and Su, Z.: Unified Optical-Thermal Four-Stream Radiative Transfer Theory for Homogeneous Vegetation Canopies, IEEE Transactions on Geoscience and Remote Sensing, 45, 1808-1822, 10.1109/TGRS.2007.895844, 2007.

Wang, W. M., Li, Z. L., and Su, H. B.: Comparison of leaf angle distribution functions: Effects on extinction coefficient and fraction of sunlit foliage, Agricultural and Forest Meteorology, 143, 106-122, 10.1016/j.agrformet.2006.12.003, 2007.

Wang, Y. and Fang, H.: Estimation of LAI with the LiDAR Technology: A Review, Remote Sensing, 12, 10.3390/rs12203457, 2020.

Weiss, M. and Baret, F.: CAN-EYE V6.4.91 User Manual, https://www6.paca.inrae.fr/can-eye/Documentation/Documentation, 2017.

Widlowski, J.-L., Côté, J.-F., and Béland, M.: Abstract tree crowns in 3D radiative transfer models: Impact on simulated open-canopy reflectances, Remote Sens. Environ., 142, 155-175, 10.1016/j.rse.2013.11.016, 2014.

Wilson, J.: Inclined point quadrats, New Phytol., 59, 1-7, 10.1111/j.1469-8137.1960.tb06195.x, 1960.

Wilson, J. W.: Analysis of the spatial distribution of foliage by two-dimensional point quadrats, New Phytol., 58, 92-99, https://doi.org/10.1111/j.1469-8137.1959.tb05340.x, 1959.

Xiao, Q., McPherson, E. G., Ustin, S. L., and Grismer, M. E.: A new approach to modeling tree rainfall interception, Journal of Geophysical Research: Atmospheres, 105, 29173-29188, 2000.

Yan, G., Jiang, H., Luo, J., Mu, X., Li, F., Qi, J., Hu, R., Xie, D., and Zhou, G.: Quantitative Evaluation of Leaf Inclination Angle Distribution on Leaf Area Index Retrieval of Coniferous Canopies, Journal of Remote Sensing, 2021, 1-15, 10.34133/2021/2708904, 2021.

You, N., Dong, J., Huang, J., Du, G., Zhang, G., He, Y., Yang, T., Di, Y., and Xiao, X.: The 10-m crop type maps in Northeast China during 2017-2019, Sci Data, 8, 41, 10.1038/s41597-021-00827-9, 2021.

Zhao, J., Li, J., Liu, Q., Xu, B., Yu, W., Lin, S., and Hu, Z.: Estimating fractional vegetation cover from leaf area index and clumping index based on the gap probability theory, International Journal of Applied Earth Observation and Geoinformation, 90, 102-112, 10.1016/j.jag.2020.102112, 2020.

Zheng, G. and Moskal, L. M.: Leaf orientation retrieval from terrestrial laser scanning (TLS) data, IEEE Transactions on Geoscience and Remote Sensing, 50, 3970-3979, 10.1109/TGRS.2012.2188533, 2012.

Zou, X. and Mõttus, M.: Retrieving crop leaf tilt angle from imaging spectroscopy data, Agricultural and Forest Meteorology, 205, 73-82, 10.1016/j.agrformet.2015.02.016, 2015.

Zou, X., Mõttus, M., Tammeorg, P., Torres, C. L., Takala, T., Pisek, J., Mäkelä, P., Stoddard, F. L., and Pellikka, P.: Photographic measurement of leaf angles in field crops, Agricultural and Forest Meteorology, 184, 137-146, 10.1016/j.agrformet.2013.09.010, 2014.